ACS APPLIED MATERIALS & INTERFACES

Research Article

www.acsami.org

Optically Tunable Chiral Plasmonic Guest–Host Cellulose Films Weaved with Long-range Ordered Silver Nanowires

Guang Chu,[†] Xuesi Wang,[‡] Tianrui Chen,[†] Jianxiong Gao,[†] Fangyuan Gai,[§] Yu Wang,*[,†] and Yan Xu*[,†]

[†]State Key Laboratory of Inorganic Synthesis and Preparative Chemistry, Jilin University, 2699 Qianjin Street, Changchun 130012, China

[‡]State Key Laboratory of Integrated Optoelectronics, College of Electronic Science and Engineering, Jilin University, 2699 Qianjin Street, Changchun 130012, China

[§]School of Petroleum and Chemical Engineering, Dalian University of Technology, 2 Dagong Road, New District of Liaodong Bay, Panjin 124221, China

Supporting Information

ABSTRACT: Plasmonic materials with large chiroptical activity at visible wavelength have attracted considerable attention due to their potential applications in metamaterials. Here we demonstrate a novel guest–host chiral nematic liquid crystal film composed of bulk self-*co*-assembly of the dispersed plasmonic silver nanowires (AgNWs) and cellulose nanocrystals (CNCs). The AgNWs-CNCs composite films show strong plasmonic optical activities, that are dependent on the chiral photonic properties of the CNCs host medium and orientation of the guest AgNWs. Tunable chiral distribution of the aligned anisotropic AgNWs with long-range order is obtained through the CNCs liquid crystal mediated realignment. The chiral plasmonic optical activity of the AgNWs-CNCs composite films can be tuned by changing the interparticle electrostatic repulsion between the CNCs nanorods and AgNWs. We also observe an electromagnetic energy transfer phenomena among the plasmonic bands of AgNWs, due to the modulation of the photonic band gap of the CNCs host matrix. This facile approach for fabricating chiral macrostructured plasmonic materials with optically tunable property is of interest for a variety of advanced optics applications.

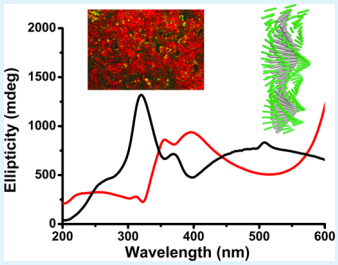

KEYWORDS: *Metamaterial, Chiroptical activity, Cellulose nanocrystals, Self-assembly, Plasmonic silver nanowires*

INTRODUCTION

The living world is asymmetrical. Chirality represents the handedness of nature by which the mirror image of an object cannot be made to coincide with itself.[1] Chiral assembly of nanoscale building blocks such as quantum dots and plasmonic metal nanoparticles into well-controlled nanoarchitectures is the key factor to the development of nanostructured metamaterials with pre-engineered macroscopic properties and promising applications in nonlinear optics,[2,3] negative refraction materials,[4] broadband circular polarizers[5] and enantioselective catalysts.[6] Various approaches have been developed for assembling nanoparticles into sophisticated two- and three-dimensional spatial geometries, such as programmed DNA origami,[7−9] amphiphile-peptide supramolecules,[10,11] templating,[12−16] polymer fiber engineering[17] and liquid crystal dispersion.[18−20] However, construction of such bulk chiroptical metamaterials from plasmonic nanoparticles by self-assembly method still remains a challenge, especially for its cost-efficient fabricating as well as the large scale production.

Being one of the most abundant renewable biopolymer on earth, cellulose can be easily derived from plants, bacterial and tunicates. Cellulose nanocrystals (CNCs), which can be obtained by controlled sulfuric acid-catalyzed degradation of bulk cellulose fibers, are currently drawing more and more interest in chemistry, physics and material science.[21] CNCs are rigid, chiral rodlike crystalline components with excellent dispersibility in water. Above a supercritical concentration, CNCs can spontaneously form a chiral nematic lyotropic liquid crystalline phase, with the rods oriented locally uniformed along a common direction.[22] Additionally, a phase transition of CNCs suspensions from chiral nematic to achiral nematic can be achieved by adding salts.[23] More interestingly, the chiral nematic order of CNCs suspension can be preserved in a condense phase upon complete drying of a thin film,[24] offering a solid macroscopic host matrix with tunable ordering for assembling guest nanoparticles, which is superior to other surfactant-based liquid crystalline counterparts in solution phase.

More recently, Kumacheva and co-workers have prepared a chiral plasmonic solid film from gold nanorods and chiral nematically ordered CNCs, exhibiting strong chiroptical activity;[25] Smalyukh et al. reported the orientationally ordered coalignment of gold nanorods in the CNCs liquid crystalline phase with polarization dependent properties.[26] These works demonstrate the extraordinary versatility of CNCs as a host

Received: February 14, 2015
Accepted: April 3, 2015
Published: April 3, 2015

DOI: 10.1021/acsami.5b01478
ACS Appl. Mater. Interfaces 2015, 7, 11863−11870

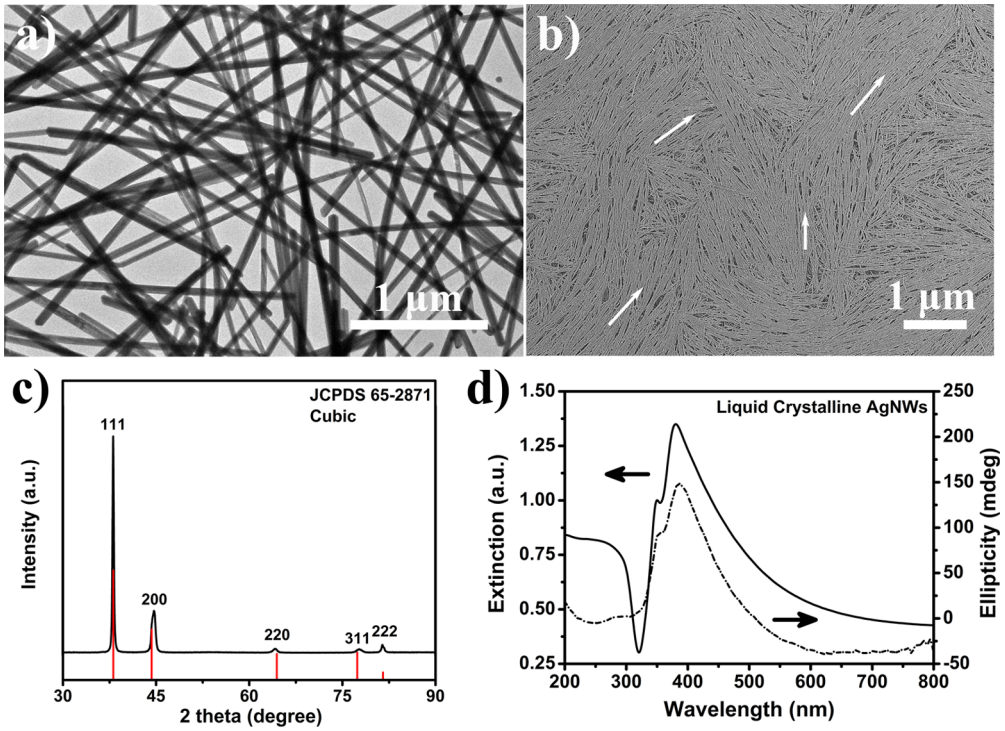

Figure 1. (a) TEM image of AgNWs, presents the uniform slender shape of the as-synthesized AgNWs. (b) SEM image of the AgNWs film, showing the direction of alignment as indicated by white arrows. (c) XRD patterns of the AgNWs, showing a well-crystallized cubic phase. (d) UV−vis and CD spectra of the liquid crystalline AgNWs colloidal suspension in water, indicating a left-handed distribution of AgNWs.

medium to construct chiral metamaterials made from anisotropic nanorods combined with liquid crystals. On the other hand, it is well-known that the spontaneous self-organization of metal nanoparticles into higher-ordered structures could afford new collective optical and optoelectronic properties, as well as various technologically significant applications.[27−29] There comes an intriguing question: can liquid crystalline CNCs modulate the assemble process of the self-patterned nanoparticles or together to make up higher-ordered structures? If the answer is yes, this will enable a simple low-cost approach to manufacture large-area (cm^2-sized) metamaterials.

By using ultralong AgNWs as building blocks, we recently reported a novel plasmonic chiral nematic metallic liquid crystal through a shape-dependent self-assembly process via van der Waals force and electrostatic interactions.[30] Pronounced surface plasmon induced circular dichroism (SPCD) signals have been observed in the colloidal suspension of AgNWs, due to the chiral woodpile-like arrangement of the AgNWs as well as the electromagnetic coupling between plasmonic AgNWs. In this work, we present a novel CNCs-based photonic material weaved with long-range ordered AgNWs, showing tunable intense chiroptical activities and yielding significant chiral anisotropy factors (g-factor) for AgNWs (up to 0.1) across the near-ultraviolet spectra range. The hybrid composite was prepared by coalignment of anisotropic liquid crystalline AgNWs dispersed in CNCs host medium followed by evaporation induced self-assembly process. In particular, we demonstrate that the photonic band gap (PBG) of chiral nematic CNCs host matrix can be used to manipulate the localized surface plasmon resonance (LSPR) features of the guest AgNWs, leading to an electromagnetic energy transfer among the LSPR bands of AgNWs over a narrow spectra range. Due to the size and density differences between the guest−host units, a concentration gradient of AgNWs occurs along the direction of gravity during evaporation, resulting in a final composite film with Janus surfaces, showing specific linear birefringence property. Furthermore, we find that the SPCD activity of the guest AgNWs can be tuned by the interparticle electrostatic repulsions between CNCs and AgNWs, resulting in a collective mirror distribution of the woodpile-like arrangement of AgNWs in CNCs films. To the best of our knowledge, this is the first report on the systematic investigation of SPCD activities of the CNCs-AgNWs composite films, which are constructed from the coalignment of two kinds of chiral nematic liquid crystalline building blocks into long-range ordering, giving rise to novel macrostructured solid films.

EXPERIMENTAL SECTION

Preparation of hybrid chiral nematic films of CNCs and AgNWs. The preparation of CNCs and AgNWs was carried out according to the reported procedures,[31,32] with the experiment details given in the Supporting Information. It is necessary to use CNCs alkaline solution to reduce the degree of sulfonation for AgNWs when they are together in solution phase. An aqueous solution of AgNWs (0.03 M) was mixed with a 3.0 wt % alkaline solution of CNCs via varying volume ratios of CNCs-to-AgNWs (Supporting Information, Table S1). The mixed solution was stirred at ambient temperature for 60 min, resulting in a homogeneous mixture. Then, the mixture was poured into polystyrene Petri dishes (60 mm), followed by evaporation under ambient conditions for 3 days, giving rise to a free-standing iridescent hybrid chiral nematic film of CNCs and AgNWs (with a thickness of ∼0.5 mm). For the purpose of comparison, the AgNWs-free chiral nematic film of CNCs was

DOI: 10.1021/acsami.5b01478
ACS Appl. Mater. Interfaces 2015, 7, 11863−11870

prepared under the same condition by using alkaline CNCs suspension only.

One more set of composite films were synthesized with same composition of CAg1a-g with respect to CNCs/AgNWs ratio and excess addition of NaCl (4 mM) to increase the ionic strength of the CNCs suspension as well as a phase transition from chiral nematic to nematic ordering (Supporting Information, Table S2). Films were dry cast in a manner that described above and designated as CAg4a-g.

RESULTS AND DISCUSSION

AgNWs with high aspect ratio were prepared by a modified polyol-reduction process based on reported procedures, in which silver nitrate solution was added dropwise into the mixture of ethylene glycol and poly(vinylpyrrolidone) at 150 °C.[31] The transmission electron microscopy (TEM) and scanning electron microscopy (SEM) images of the AgNWs are shown in Figure 1a, b, respectively. The as-synthesized AgNWs have an average length of 7.5 μm and an average diameter of 110 nm (Figure 1a), with the calculated aspect ratio of 68.2. A partial close-packed nematic arrangement of AgNWs with multilayer ordering is observed, which can be identified as layer-by-layer stacking of ribbon-like AgNWs superstructures (Figure 1b). Such an ordering occurs only when the concentration of AgNWs suspension is above a critical value to maximize the entropy of the self-patterned structure by minimizing the excluded volume per AgNWs in the arrays.[33] The XRD pattern of AgNWs is presented in Figure 1c. The peaks at 38.1°, 45.6°, 64.3°, 77.6° and 81.6° can be indexed to (111), (200), (220), (311) and (222) reflections of a cubic phase (JCPDS 87−0720), confirming the crystalline nature of AgNWs. The UV−vis spectrum of AgNWs colloidal suspension shows a series of LSPR bands, among which the two strong peaks at 380 and 350 nm can be attributed to the coupling of in-plane dipole and quadrupole plasmon resonances, respectively (Figure 1d, left).[34] And the corresponding CD spectrum of the liquid crystalline AgNWs shows two positive SPCD peaks at 385 and 353 nm, with a maximum g-factor of 0.0034, indicating a left-handed chiral distribution of AgNWs in water (Figure 1d, right).[30]

The CNCs we used are prepared by sulfuric acid hydrolysis of a commercial fully bleached cotton pulp, showing rod morphology with an average length and diameter around 300 and 15 nm, respectively (Figure S1). First, we have tested the phase behavior of CNCs-AgNWs dispersion by drop-casting the mixture into a liquid crystal cell and the evaporation process is tracked by polarized optical microscopy (POM). The initial concentrations of CNCs and AgNWs used in the mixture are below the critical concentration for anisotropic phase formation, but the drop appears discrete AgNWs in dispersions (Figure 2a), no aggregation occurs. The dispersions are isotropic at first, but with increasing concentration (evaporation), two kinds of textures are established, demonstrating the formation of liquid crystalline phase. Figure 2b is the POM image of AgNWs liquid crystal in CNCs host suspension, a coffee-ring like texture is observed indicating the formation of chiral nematic arrangement of AgNWs. As the evaporation proceeds, obvious fingerprint texture belongs to CNCs is observed, indicating the formation of chiral nematic phase of CNCs as well (Figure 2c). Upon complete evaporation of water from the mixture, a composite film of CNCs-AgNWs is obtained with strong bright birefringent band, indicating the retention of chiral nematic structure (Figure 2d).

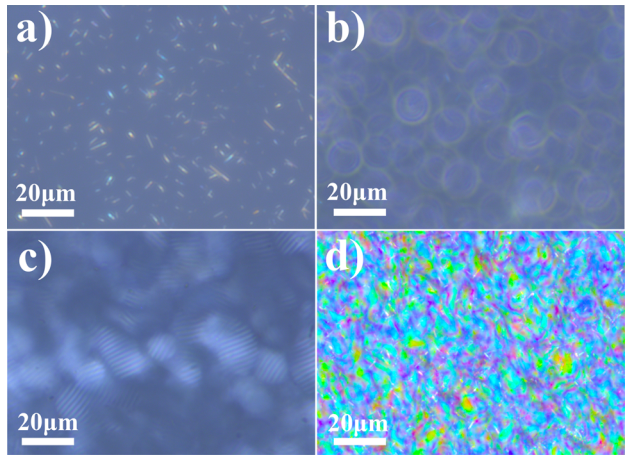

Figure 2. POM images of a drop taken from CNCs-AgNWs during evaporation in liquid crystal cell. (a) POM image of an isotropic phase of the CNCs-AgNWs mixture, showing discrete AgNWs. (b) POM image of the anisotropic phase of AgNWs in mixture with a coffee-ring like texture. (c) POM image of the anisotropic phase of CNCs in mixture with fingerprint texture. (d) The resulting CNCs-AgNWs composite film with strong birefringent textures. All the images were taken under cross-polarized light.

The hybrid chiral nematic films of CNCs-AgNWs (designated as CAg films) are prepared from 3.0 wt % aqueous alkaline suspension of CNCs and 0.03 M colloidal suspension of AgNWs at varying volume ratios via evaporation-induced self-assembly approach at room temperature (Table S1). Figure 3a is the Focused-ion-beam (FIB) image cut of the sample CAg3e with oblique view of the film. It is obvious that the image can be divided into three parts: the interface between air and CNCs film (district A), the intersection of AgNWs and CNCs rods (district B), and an extensive periodic structure of

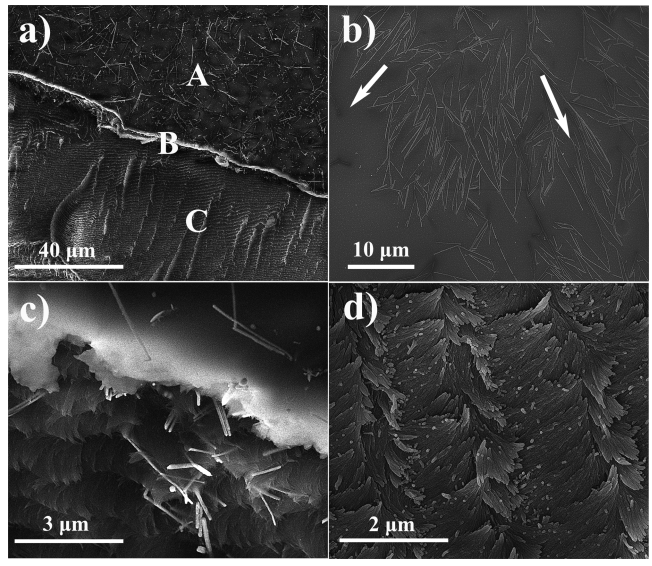

Figure 3. FIB images of the chiral nematic CAg film. (a) Oblique view of a cracked sample of CAg3e with three different districts. (b) Top view of the surface film shows a nematic like arrangement of the guest AgNWs. The arrow is the direction of the AgNWs orientation. (c) Side view of the intersection of AgNWs and CNCs host matrix. (d) Magnified FIB image of CAg3e showing a left-handed chiral arrangement of the host CNCs rods.

DOI: 10.1021/acsami.5b01478
ACS Appl. Mater. Interfaces 2015, 7, 11863−11870

the aligned CNCs rods (district C). On the surface of the CNCs films (district A), a nematic arrangement of AgNWs is observed (Figure 3b), similar to that of the pure AgNWs film (Figure 1b), indicating the nematic alignment of AgNWs in CNCs host matrix. Figure 3c is the magnified FIB image of district B, some vertical and lateral gaps of AgNWs are observed within the CNCs host matrix, which could form a lot of junctions of AgNWs. District C shows an anticlockwise twisting morphology with typical layered structure and rod-like texture, indicating a left-handed helical organization which is responsible for the selective reflection of left-handed circularly polarized light (Figure 3d).[35]

In chiral nematic cellulose film, it is well-known that the position of PBG is optically tunable from visible to near-infrared regions by changing the electrostatic repulsions between individual CNCs nanorods.[36,37] Therefore, the relative question naturally arises as to whether we may manipulate the LSPR properties of AgNWs by altering the PBG positions of the CNCs host matrix. To answer this question, three series of CNCs-AgNWs composite films with the same AgNWs contents, and different PBG position centered at 295, 546, and 698 nm, respectively (Figure 4), are used as ideal samples

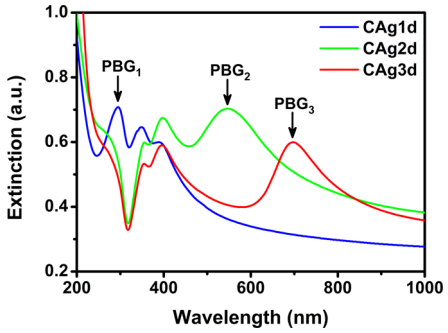

Figure 4. UV−vis spectra of the CAg sample, showing the modulation of LSPR properties of AgNWs by varying the PBG of the CNCs host matrix.

to study the effect of PBG on LSPR bands of AgNWs. The two main LSPR peaks of AgNWs in CNCs host matrix are centered at 398 and 356 nm, which are slightly shifted to longer wavelengths in contrast to the liquid crystalline AgNWs in water (Figure 1d). This is a result of the increase of medium refractive index (n) from that of water (n = 1.33) to CNCs (n = 1.56). As it can be seen from CAg 3d with its PBG positioned far away from the LSPR peaks of AgNWs, which can be used as a reference. Besides that, the LSPR peaks of CAg1d and CAg2d show a significant difference due to the positions of their corresponding PBG, comparing with that of CAg3d. For CAg2d whose LSPR lies at the blue end of PBG, the LSPR intensity is stronger than that of CAg3d, despite the same contents of AgNWs they have. More interestingly, for CAg1d whose LSPR lies at the red end of its PBG, the LSPR intensity at 356 nm is stronger than that at 398 nm, implying the occurrence of surface electromagnetic energy transfer between the LSPR bands. Surface electromagnetic waves in PBG and surface plasmons in AgNWs are both nonradiative modes which can be coupled directly in CNCs matrix. When the frequencies of LSPR is at the edges of PBG, the surface plasmon mode dispersion is flat and the density of state of the surface plasmon mode is high, resulting in a high field enhancement close to the metal surface,[38] and a selective modulation of the LSPR bands of AgNWs. However, with the increasing of AgNWs contents, the PBG induced abnormal LSPR effect weakens and eventually disappear (Figure S2), indicating a concentration dependent effect. This phenomenon may be due to the high loading of AgNWs in hybrid composite, resulting in signal distortion at AgNWs LSPR bands. Furthermore, it is also possible to deduce a suitable loading range of AgNWs from the UV−vis spectra (0.1−1 mL AgNWs/5 mL CNCs), thus, the limitation of this material can be easily obtained.

POM images of the CAg films show a mass of birefringent textures with a red-colored shift relative to the bulk hybrid composites, indicating a typical anisotropy of the host materials (Figure 5a-c). And it should be pointed out that, due to the

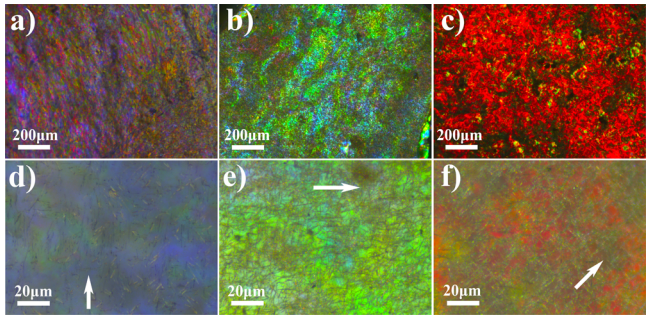

Figure 5. POM images of the chiral nematic CAg films: (a) CAg1g, (b) CAg2g, (c) CAg3g, respectively, showing optically tunable blue to red iridescence. (d)-(f) are the magnified POM images of the corresponding CAg films, showing a partially collective nematic-like orientation of AgNWs in the birefringent CNCs host matrix. The arrow indicates the direction of AgNWs collective orientation.

large size of the guest AgNWs, the collective orientation and distribution of AgNWs can be discriminated. As shown in the high magnification POM images in Figure 5d-f, different collective orientations of the AgNWs are observed in the host CNCs matrix. The slender AgNWs are clearly seen with ordered nematic like distribution, further demonstrating that the formation of AgNWs chiral nematic liquid crystalline structure is under the guidance of CNCs nanorods, instead of spontaneous aggregation during evaporation.

The strength of the chiroptical activity as well as the chiral distribution in multilayer AgNWs superstructure both are critically depending on the concentration of the guest AgNWs in host CNCs matrix (Figure S3). For verification, we choose the CAg film with the highest AgNWs concentration as representative to study the SPCD properties of the hybrid films. It is well-known that the oriented films with macroscopic anisotropy can exhibit both linear dichroism and birefringence properties, measurements such as the CD spectroscopy can show artifacts from the linear anisotropy.[39] The linear dichroism possibility of the CAg samples can be eliminated by measuring at various azimuthal orientations perpendicular to the light beam, finding that the spectra remain literally the same (Figure S4). However, due to the differences in size and density between CNCs and AgNWs, a gravity-assisted concentration gradient of AgNWs occurs during the evaporation process, resulting in the final hybrid film with Janus side, thus, for these films, the front side which has less amount of AgNWs than the back side (Figure S5). A series of dedicated tests of the "front-and-back" CD measurements of the CAg samples and corresponding g-factors are presented in Figure 6 (the

DOI: 10.1021/acsami.5b01478
ACS Appl. Mater. Interfaces 2015, 7, 11863−11870

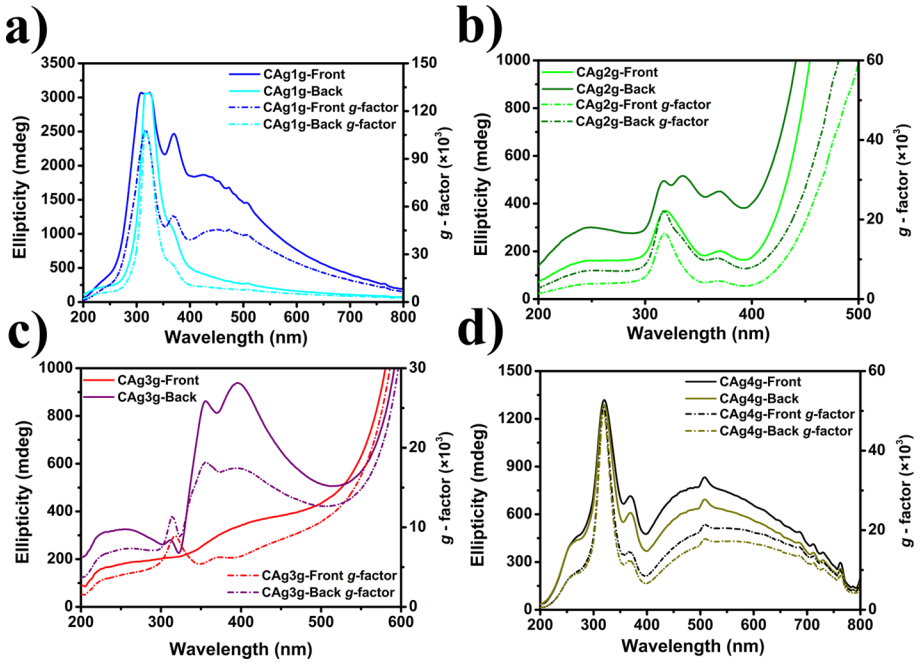

Figure 6. (a)-(d) are the ensemble CD spectra (solid line) and corresponding g-factor (dotted line) of the CAg hybrid films, which measured by flipping the same films with both front and back sides normal to the beam path, indicating strong linear birefringence and structure-dependent LSPR properties. The thickness of these films we used is about 0.5 mm.

complete CD spectra and corresponding UV−vis spectra are shown in Figure S6, Figure S7). It is notable that significant differences between the front and back side of the same film are observed in all samples, indicating a strong linear birefringence of these films. For CAg1g, the SPCD intensity of the guest AgNWs is stronger when measured in front side than that measured in back side with a maximum g-factor of 0.108 (Figure 6a). For CAg2g, the shape and intensity of SPCD measured at the back side is similar to that of the front side, but with a new peak at 336 nm. And it is interesting to note that this new peak disappears in related g-factors (Figure 6b). Intriguing, the SPCD spectra of CAg3g are totally different from CAg1g and CAg2g (Figure 6c). The SPCD intensity measured in back side is stronger than that in front side, instead, with its shape similar to that of the AgNWs chiral nematic liquid crystalline phase measured in water (Figure 1d). This linear birefringence of the chiral nematic CAg films indicates a unique macroscopic anisotropy in solid state.[40] What is the most interesting is that the SPCD linear birefringence vanishes when the CNCs host matrix is in a nematic ordering (Figure 6d, the corresponding SEM and POM images are shown in Figure S8, S9), thus, the SPCD signals of the nematic CAg4g film remain constant when it is measured in both front and back sides. These results confirm the strong structure-dependent chiroptical response in the CAg hybrid films. The structural variation of CNCs host matrix has strong impact on the SPCD response of the chiral hybrid films. Thus, the helical arrangement of the host CNCs nanorods could induce a linear birefringence of the guest AgNWs, while the achiral nematic arrangement of CNCs is not.

Further investigation shows that the SPCD optical activity of the hybrid composite films can be modulated by varying the interparticle electrostatic repulsions between the CNCs rods and slender AgNWs. The surface state of CNCs and AgNWs can be quantified by measuring the zeta potential and Z-average size of their own suspension. As shown in Table S3, both CNCs and AgNWs are negatively charged with strong electrostatic repulsions between them, so that the mixed suspension is stable and aggregation will not happen. As an indicator of electrostatic repulsion, the surface charge density of CNCs is reduced from 0.71 to 0.45 e·nm^{-2}, therefore, the higher the surface charge density is, the stronger the electrostatic repulsion becomes. As described by previous reports, the acid hydrolysis used to extract CNCs from bulk cellulose fibrils is performed at very high concentration, leading to the sulfate ester groups and protons impart to the cellulose chains at the surface of CNCs nanorods.[41] Ultrasonic energy treatment of the negatively charged CNCs suspension drives out some of the ions trapped in the bound-water layer of CNCs nanorods, thereby forming a stronger electrical double layer and weaker chiral interactions or electrostatic repulsions between CNCs nanorods, leading to a larger helical pitch in the resulting solid chiral nematic films.[36] Moderate ionic strength could shield the surface charge and reduce the effect of electrostatic repulsion.[23,42] However, upon the addition of an excessive amount of salt in CNCs suspension, the excess cations will interact with the surface of CNCs rods, resulting in an increase in electrostatic repulsions. And the twisting power between electrolytes will impede the ordering of the charged CNCs nanorods, leading to a phase transition in CNCs suspension from chiral nematic to achiral nematic ordering.

Figure 7 is the CD spectra of the CAg films measured at their back surface of the films perpendicularly to the beam path. For CAg3g with the smallest interparticles electrostatic repulsion, the SPCD signal is similar to that of chiral nematically ordered AgNWs liquid crystal measured in water, except for a slight shift to longer wavelength, suggesting a left-handed chiral collective distribution of AgNWs in CNCs host matrix. It shows three LSPR peaks at 312, 356, and 396 nm and two dips at 320 and 370 nm, respectively. However, a clear change in the CD signal is observed as a result of increasing the electrostatic repulsion between host CNCs nanorods and guest AgNWs. For CAg1g

DOI: 10.1021/acsami.5b01478
ACS Appl. Mater. Interfaces 2015, 7, 11863−11870

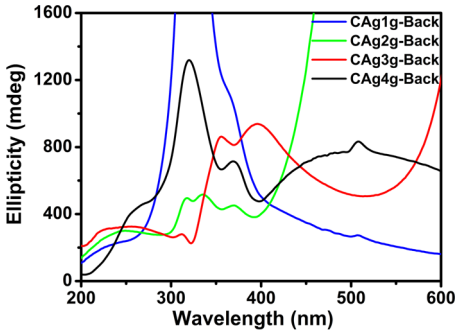

Figure 7. CD spectra of the hybrid CAg films, with their back sides facing normal to the beam path.

and CAg2g, a partially mirrored SPCD signal is observed comparing with CAg3g. Due to the significant linear birefringence effect, the SPCD signal of CAg2g measured from the back side shows three dips at 324, 356, 396 nm, and three peaks at 320, 335, and 370 nm, respectively. The corresponding SPCD signal of CAg1g shows a shoulder at the range of 356 to 400 nm, which can be assigned to the LSPR bands of AgNWs. Additionally, this phase reversal phenomenon is even more obviously for CAg1g and CAg2g based on the SPCD signals measured with the front side normal to the beam path (Figure S10). It was considered at first that the SPCD optical activity in the sample of CAg1g, CAg2g and CAg3g may be derived from the chiral ordering of the host matrix, because the electromagnetic wave polarization and propagation inside the chiral nematic structure is peculiar, the periodic modulation of the refractive index modifies the dispersion relationship of surface plasmons propagation.[38,43] However, CAg4g with a nematic ordering of the host matrix and the strongest interparticle electrostatic repulsion shows a completely opposite scenario, with two peaks at 320 and 370 nm, and two dips at 356 and 396 nm, respectively, in contrast to CAg3g. This additional result suggests that the SPCD signal originates from the chiral assembly of AgNWs, instead of the chiral environment of the CNCs host matrix. Previous theoretical study has shown that the structure and configuration of the plasmonic nanostructures strongly affect the plasmon coupling within the nanostructure as well as the corresponding chiroptical activity.[44,45] It is therefore reasonable to deduce that the SPCD signal arises from the interactions of chiral nematically ordered AgNWs, and the progressive flipping of the SPCD signal of the CAg film could indicate a collective mirrored chiral distribution of AgNWs in the CNCs host matrix.

On the basis of the above-mentioned results, an artistic depiction of the possible approach about the realignment of guest AgNWs in CNCs host matrix is illustrated in Scheme 1. The chiral self-*co*-alignment of AgNWs in CNCs suspension above a critical concentration is driven by the minimization of free energy in the system ($\Delta G = \Delta H\text{-}T\Delta S$).[27,33,46] In this system, the enthalpy (ΔH) component can be attributed to the interactions between guest−host building blocks while the entropy (ΔS) represents the free volume (orientation) of each building unit. And the interactions between AgNWs and CNCs are typically governed by van der Waals interaction and electrostatic repulsion, respectively. When the electrostatic repulsion among CNCs nanorods is small, the guest AgNWs has tendency to spontaneously form a left-handed chiral distribution, the same way as AgNWs dispersed in water.

Scheme 1. Schematic illustration of the self-assembly approach of CNCs and AgNWs with electrostatic repulsion induced realignment

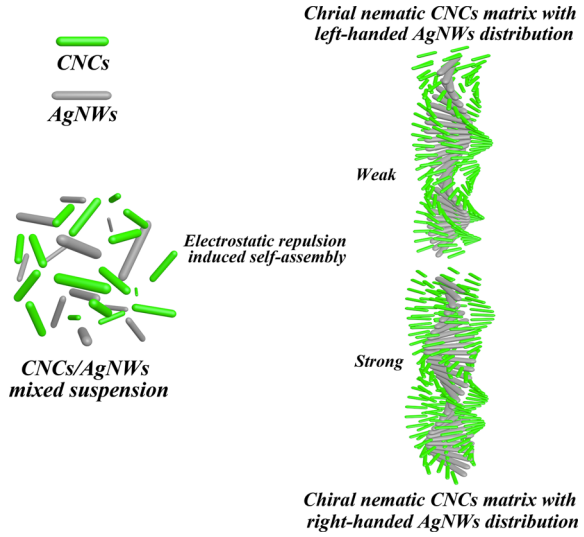

However, with the increasing of electrostatic repulsion between the guest−host building blocks, in this instance, a gradual transition from the left-handed distribution to the right-handed distribution of AgNWs occurs in order to gain more free volume for each AgNWs and minimize the total free energy in the system, tending to form a close-packed chiral woodpile-like arrangement of AgNWs dependent on their slender shape. The corresponding CD spectra indicate that when the mixed suspension of AgNWs and CNCs is dried to form a solid film, the drying process does not disturb the interparticle interaction between the guest−host building blocks, and the sophisticated architecture of the hybrid film can be preserved.

CONCLUSION

In conclusion, we have demonstrated the plasmonic guest−host CNCs mediated oriented coalignment of AgNWs hybrid system, which can be engineered for manipulating the surface plasmon propagation in near-ultraviolet spectra ranges by using the corresponding PBG. This ordered film of anisotropic AgNWs in chiral nematic or nematic CNCs host matrix is enabled by controlled weak electrostatic repulsion between the CNCs nanorods and the AgNWs, leading to a collective mirrored chiral distribution of AgNWs. Unlike the complex and expensive "top-down" method (electron beam-, scanning probe- and photo- lithography technique), our strategy shows great potential for future metamaterials designing with cost-effective and eco-friendly procedure, and it can also be applied to other kind of self-organized nanoparticle-based system, such as quantum dots, magnetic and rare earth up-conversion nanorods, and so on. The ease of fabrication and scalability of the method combined with significant and tunable SPCD and LSPR property makes the ordered CAg films particularly attractive as promising candidates for advanced optics applications such as novel orientation sensors and mirrorless lasing. In addition, as a kind of homochiral photonic crystal, the Raman optical activity of the CAg hybrid composite should be interesting, it deserves further investigation for chiral recognition.[47]

DOI: 10.1021/acsami.5b01478
ACS Appl. Mater. Interfaces 2015, 7, 11863−11870

■ ASSOCIATED CONTENT

Supporting Information

Additional experimental details and figures (such as POM, TEM, UV−vis spectra and CD spectra) as well as charts are demonstrated in Supporting Information. This material is available free of charge via the Internet at http://pubs.acs.org.

■ AUTHOR INFORMATION

Corresponding Authors

* Email: yanxu@jlu.edu.cn.
*Email: wangyu@jlu.edu.cn.

Author Contributions

G. C. synthesized the CNCs-AgNWs composite films and carried out the FIB, POM, CD and UV−vis measurements. X. W. supplied the AgNWs and contributed valuable expertise on chiral nematic liquid crystalline AgNWs. G. C. designed and led the project. The manuscript was written through contributions of all authors. All authors have given approval to the final version of the manuscript.

Notes

The authors declare no competing financial interest.

■ ACKNOWLEDGMENTS

The authors are grateful to the funding agencies including the National Natural Science Foundation of China (21171067, 21373100), Jilin Provincial Talent Funds (802110000412) and Tang Aoqing Professor Funds of Jilin University (450091105161). Sincere gratitude goes to Professor Xiao-An Zhang for POM imaging analysis.

■ REFERENCES

(1) Welch, C. J. Chirality in the Natural World: Life through the Looking Glass. *Chirality in the Natural and Applied Sciences. Oxford: Blackwell* **2002**, 285−302.

(2) Rodrigues, S. P.; Lan, S.; Kang, L.; Cui, Y.; Cai, W. Nonlinear Imaging and Spectroscopy of Chiral Metamaterials. *Adv. Mater.* **2014**, *26*, 6157−6162.

(3) Zhang, X.; Luo, W.; Wang, L. J.; Jiang, W. Third-Order Nonlinear Optical Vitreous Material Derived from Mesoporous Silica Incorporated with Au Nanoparticles. *J. Mater. Chem. C* **2014**, *2*, 6966−6970.

(4) Valev, V. K.; Baumberg, J. J.; Sibilia, C.; Verbiest, T. Chirality and Chiroptical Effects in Plasmonic Nanostructures: Fundamentals, Recent Progress, and Outlook. *Adv. Mater.* **2013**, *25*, 2517−2534.

(5) Gansel, J. K.; Thiel, M.; Rill, M. S.; Decker, M.; Bade, K.; Saile, V.; Von Freymann, G.; Linden, S.; Wegener, M. Gold Helix Photonic Metamaterial as Broadband Circular Polarizer. *Science* **2009**, *325*, 1513−1515.

(6) Tamura, M.; Fujihara, H. Chiral Bisphosphine Binap-Stabilized Gold and Palladium Nanoparticles with Small Size and Their Palladium Nanoparticle-Catalyzed Asymmetric Reaction. *J. Am. Chem. Soc.* **2003**, *125*, 15742−15743.

(7) Li, Z.; Zhu, Z.; Liu, W.; Zhou, Y.; Han, B.; Gao, Y.; Tang, Z. Reversible Plasmonic Circular Dichroism of Au Nanorod and DNA Assemblies. *J. Am. Chem. Soc.* **2012**, *134*, 3322−3325.

(8) Lan, X.; Chen, Z.; Dai, G.; Lu, X.; Ni, W.; Wang, Q. Bifacial DNA Origami-Directed Discrete, Three-Dimensional, Anisotropic Plasmonic Nanoarchitectures with Tailored Optical Chirality. *J. Am. Chem. Soc.* **2013**, *135*, 11441−11444.

(9) Dai, G.; Lu, X.; Chen, Z.; Meng, C.; Ni, W.; Wang, Q. DNA Origami-Directed, Discrete Three-Dimensional Plasmonic Tetrahedron Nanoarchitectures with Tailored Optical Chirality. *ACS Appl. Mater. Interfaces* **2014**, *6*, 5388−5392.

(10) George, J.; Thomas, K. G. Surface Plasmon Coupled Circular Dichroism of Au Nanoparticles on Peptide Nanotubes. *J. Am. Chem. Soc.* **2010**, *132*, 2502−2503.

(11) Song, C.; Blaber, M. G.; Zhao, G.; Zhang, P.; Fry, H. C.; Schatz, G. C.; Rosi, N. L. Tailorable Plasmonic Circular Dichroism Properties of Helical Nanoparticle Superstructures. *Nano Lett.* **2013**, *13*, 3256−3261.

(12) Chu, G.; Xu, W.; Qu, D.; Wang, Y.; Song, H.; Xu, Y. Chiral Nematic Mesoporous Films of Y_2O_3:Eu^{3+} with Tunable Optical Properties and Modulated Photoluminescence. *J. Mater. Chem. C* **2014**, *2*, 9189−9195.

(13) Chu, G.; Feng, J.; Wang, Y.; Zhang, X.; Xu, Y.; Zhang, H. J. Chiral Nematic Mesoporous Films of ZrO_2:Eu^{3+}: New Luminescent Materials. *Dalton Trans.* **2014**, *43*, 15321−15327.

(14) Schlesinger, M.; Giese, M.; Blusch, L. K.; Hamad, W. Y.; MacLachlan, M. J. Chiral Nematic Cellulose-Gold Nanoparticle Composites from Mesoporous Photonic Cellulose. *Chem. Commun.* **2015**, *51*, 530−533.

(15) Qi, H.; Shopsowitz, K. E.; Hamad, W. Y.; MacLachlan, M. J. Chiral Nematic Assemblies of Silver Nanoparticles in Mesoporous Silica Thin Films. *J. Am. Chem. Soc.* **2011**, *133*, 3728−3731.

(16) Campbell, M. G.; Liu, Q.; Sanders, A.; Evans, J. S.; Smalyukh, I. I. Preparation of Nanocomposite Plasmonic Films Made from Cellulose Nanocrystals or Mesoporous Silica Decorated with Unidirectionally Aligned Gold Nanorods. *Materials* **2014**, *7*, 3021−3033.

(17) Jung, S. H.; Jeon, J.; Kim, H.; Jaworski, J.; Jung, J. H. Chiral Arrangement of Achiral Au Nanoparticles by Supramolecular Assembly of Helical Nanofiber Templates. *J. Am. Chem. Soc.* **2014**, *136*, 6446−6452.

(18) Liu, Q.; Senyuk, B.; Tang, J.; Lee, T.; Qian, J.; He, S.; Smalyukh, I. I. Plasmonic Complex Fluids of Nematiclike and Helicoidal Self-Assemblies of Gold Nanorods with a Negative Order Parameter. *Phys. Rev. Lett.* **2012**, *109*, 088301.

(19) Liu, Q.; Yuan, Y.; Smalyukh, I. I. Electrically and Optically Tunable Plasmonic Guest-Host Liquid Crystals with Long-Range Ordered Nanoparticles. *Nano Lett.* **2014**, *14*, 4071−4077.

(20) Liu, Q.; Cui, Y.; Gardner, D.; Li, X.; He, S.; Smalyukh, I. I. Self-Alignment of Plasmonic Gold Nanorods in Reconfigurable Anisotropic Fluids for Tunable Bulk Metamaterial Applications. *Nano Lett.* **2010**, *10*, 1347−1353.

(21) Habibi, Y.; Lucia, L. A.; Rojas, O. J. Cellulose Nanocrystals: Chemistry, Self-Assembly, and Applications. *Chem. Rev.* **2010**, *110*, 3479−3500.

(22) Revol, J. F.; Bradford, H.; Giasson, J.; Marchessault, R.; Gray, D. Helicoidal Self-Ordering of Cellulose Microfibrils in Aqueous Suspension. *Int. J. Biol. Macromol.* **1992**, *14*, 170−172.

(23) Dong, X. M.; Kimura, T.; Revol, J. F.; Gray, D. G. Effects of Ionic Strength on the Isotropic-Chiral Nematic Phase Transition of Suspensions of Cellulose Crystallites. *Langmuir* **1996**, *12*, 2076−2082.

(24) Revol, J. F.; Godbout, L.; Gray, D. Solid Self-Assembled Films of Cellulose with Chiral Nematic Order and Optically Variable Properties. *J. Pulp Pap. Sci.* **1998**, *24*, 146−149.

(25) Querejeta-Fernández, A.; Chauve, G.; Methot, M.; Bouchard, J.; Kumacheva, E. Chiral Plasmonic Films Formed by Gold Nanorods and Cellulose Nanocrystals. *J. Am. Chem. Soc.* **2014**, *136*, 4788−4793.

(26) Liu, Q.; Campbell, M. G.; Evans, J. S.; Smalyukh, I. I. Orientationally Ordered Colloidal Co-Dispersions of Gold Nanorods and Cellulose Nanocrystals. *Adv. Mater.* **2014**, *26*, 7178−7184.

(27) Kim, F.; Kwan, S.; Akana, J.; Yang, P. Langmuir-Blodgett Nanorod Assembly. *J. Am. Chem. Soc.* **2001**, *123*, 4360−4361.

(28) Mitov, M.; Portet, C.; Bourgerette, C.; Snoeck, E.; Verelst, M. Long-Range Structuring of Nanoparticles by Mimicry of a Cholesteric Liquid Crystal. *Nat. Mater.* **2002**, *1*, 229−231.

(29) Huang, J.; Kim, F.; Tao, A. R.; Connor, S.; Yang, P. Spontaneous Formation of Nanoparticle Stripe Patterns through Dewetting. *Nat. Mater.* **2005**, *4*, 896−900.

(30) Wang, X.; Zou, Y.; Zhu, J.; Wang, Y. Silver Cholesteric Liquid Crystalline: Shape-Dependent Assembly and Plasmonic Chiroptical Response. *J. Phys. Chem. C* **2013**, *117*, 14197−14205.

(31) Jiu, J.; Araki, T.; Wang, J.; Nogi, M.; Sugahara, T.; Nagao, S.; Koga, H.; Suganuma, K.; Nakazawa, E.; Hara, M. Facile Synthesis of

DOI: 10.1021/acsami.5b01478
ACS Appl. Mater. Interfaces 2015, 7, 11863−11870

Very-Long Silver Nanowires for Transparent Electrodes. *J. Mater. Chem. A* **2014**, *2*, 6326−6330.
(32) Beck-Candanedo, S.; Viet, D.; Gray, D. G. Induced Phase Separation in Low-Ionic-Strength Cellulose Nanocrystal Suspensions Containing High-Molecular-Weight Blue Dextrans. *Langmuir* **2006**, *22*, 8690−8695.
(33) Onsager, L. The Effects of Shape on the Interaction of Colloidal Particles. *Ann. N.Y. Acad. Sci.* **1949**, *51*, 627−659.
(34) Rycenga, M.; Cobley, C. M.; Zeng, J.; Li, W.; Moran, C. H.; Zhang, Q.; Qin, D.; Xia, Y. Controlling the Synthesis and Assembly of Silver Nanostructures for Plasmonic Applications. *Chem. Rev.* **2011**, *111*, 3669−3712.
(35) Dumanli, A. G.; Kamita, G.; Landman, J.; van der Kooij, H.; Glover, B. J.; Baumberg, J. J.; Steiner, U.; Vignolini, S. Controlled, Bio-Inspired Self-Assembly of Cellulose-Based Chiral Reflectors. *Adv. Opt. Mater.* **2014**, *2*, 646−650.
(36) Beck, S.; Bouchard, J.; Berry, R. Controlling the Reflection Wavelength of Iridescent Solid Films of Nanocrystalline Cellulose. *Biomacromolecules* **2010**, *12*, 167−172.
(37) Lagerwall, J. P. F.; Schutz, C.; Salajkova, M.; Noh, J.; Park, J. H.; Scalia, G.; Bergstrom, L. Cellulose Nanocrystal-Based Materials: From Liquid Crystal Self-Assembly and Glass Formation to Multifunctional Thin Films. *NPG Asia Mater.* **2014**, *6*, e80.
(38) Barnes, W. L.; Dereux, A.; Ebbesen, T. W. Surface Plasmon Subwavelength Optics. *Nature* **2003**, *424*, 824−830.
(39) Yeom, B.; Zhang, H.; Zhang, H.; Park, J. I.; Kim, K.; Govorov, A. O.; Kotov, N. A. Chiral Plasmonic Nanostructures on Achiral Nanopillars. *Nano Lett.* **2013**, *13*, 5277−5283.
(40) Frank, B.; Yin, X.; Schäferling, M.; Zhao, J.; Hein, S. M.; Braun, P. V.; Giessen, H. Large-Area 3D Chiral Plasmonic Structures. *ACS Nano* **2013**, *7*, 6321−6329.
(41) Beck-Candanedo, S.; Roman, M.; Gray, D. G. Effect of Reaction Conditions on the Properties and Behavior of Wood Cellulose Nanocrystal Suspensions. *Biomacromolecules* **2005**, *6*, 1048−1054.
(42) Pan, J.; Hamad, W.; Straus, S. K. Parameters Affecting the Chiral Nematic Phase of Nanocrystalline Cellulose Films. *Macromolecules* **2010**, *43*, 3851−3858.
(43) Yeh, P.; Gu, C. *Optics of Liquid Crystal Displays*; John Wiley & Sons, 2010; Vol. *67*.
(44) Fan, Z.; Govorov, A. O. Plasmonic Circular Dichroism of Chiral Metal Nanoparticle Assemblies. *Nano Lett.* **2010**, *10*, 2580−2587.
(45) Fan, Z.; Govorov, A. O. Helical Metal Nanoparticle Assemblies with Defects: Plasmonic Chirality and Circular Dichroism. *J. Phys. Chem. C* **2011**, *115*, 13254−13261.
(46) Gong, J.; Li, G.; Tang, Z. Self-Assembly of Noble Metal Nanocrystals: Fabrication, Optical Property, and Application. *Nano Today* **2012**, *7*, 564−585.
(47) Huang, Y.; Fang, Y.; Zhang, Z.; Zhu, L.; Sun, M. Nanowire-Supported Plasmonic Waveguide for Remote Excitation of Surface-Enhanced Raman Scattering. *Light: Sci. Appl.* **2014**, *3*, e199.

DOI: 10.1021/acsami.5b01478
ACS Appl. Mater. Interfaces 2015, 7, 11863−11870